Toxoplasma F-Box Protein 1 is Required for Daughter Cell Scaffold Function During Parasite Replication

Carlos G. Baptista[a], Agnieszka Lis[a], Bowen Deng[b], Ashley Dittmar[a*], Christopher M. West[b], and Ira J. Blader[a#]

[a]Department of Microbiology and Immunology, University at Buffalo School of Medicine, Buffalo, NY 14203

[b]Department of Biochemistry & Molecular Biology, University of Georgia, Athens, GA 30602 USA

[#] Address correspondence to: iblader@buffalo.edu

* Current Address: HarkerBIO, LLC, 700 Ellicott St, Buffalo, NY 14203

Running Title: *Toxoplasma* F-Box Protein Functions in Endodyogeny

Keywords: Cell Cycle, Parasitology, Ubiquitin, Membrane Trafficking, Cytoskeleton

ABSTRACT

F-box proteins bind to the adaptor protein Skp1 and serve as substrate receptors for the Skp1, Cullin, F-box E3 ubiquitin ligase complex. F-box proteins therefore regulate critical cellular processes including cell cycle progression and membrane trafficking. While F-box proteins are conserved throughout eukaryotes and are well studied in yeast and mammals, studies in parasitic protozoa are lagging. We have identified seventeen putative F-box proteins in the *Toxoplasma* genome of which four have predicted homologs in *Plasmodium*. Two of the conserved F-box proteins were demonstrated to be important for *Toxoplasma* fitness and here we focus on an F-box protein, named TgFBXO1, because it is the most highly expressed by replicative tachyzoites and was also identified in an interactome screen as a *Toxoplasma* SKP1 binding protein. TgFBXO1 interacts with *Toxoplasma* SKP1 confirming it as a bona fide F-box protein. In interphase parasites, TgFBXO1 is a component of the Inner Membrane Complex (IMC), which is an organelle that underlies the plasma membrane. Early during replication, TgFBXO1 relocalizes to the developing daughter cell scaffold, which is the site where the daughter cell IMC and microtubules form and extend from. TgFBXO1 relocalization required centrosome duplication but occurred before duplication of the centrocone, which is the nuclear envelope embedded spindle compartment. Daughter cell scaffold localization required N-myristoylation of TgFBXO1 and was dependent on the small molecular weight GTPase, TgRab11b. Finally, we demonstrate that TgFBXO1 is required for parasite growth due to its function as a daughter cell scaffold effector. TgFBXO1 is the first F-box protein to be studied in apicomplexan parasites and represents the first protein demonstrated to be important for daughter cell scaffold function.

44

AUTHOR SUMMARY

Toxoplasma gondii is a protozoan parasite that can cause devastating and life threatening disease in immunocompromised patients and in fetuses. Its replication is important to study because it is the primary reason that toxoplasmosis patients develop disease. The parasite replicates by a unique process named endodyogeny in which two daughter parasites develop within the mother cell. Early during this process the parasite creates a structure called the Daughter Cell Scaffold whose function is to serve as the site from which the new parasite will form from. Here, we report the identification of one of the first proteins recruited to the Daughter Cell Scaffold and its importance in executing its function.

55 **INTRODUCTION**

56 *Toxoplasma gondii* is an intracellular apicomplexan parasite responsible for one of
57 the most common parasitic infections in humans and animals [1, 2]. Infections are
58 initiated by digesting either bradyzoite-containing tissue cysts or sporozoite-laden oocysts
59 that are disrupted in the stomach [3]. Released parasites then infect the small intestine
60 and convert into tachyzoites, which triggers the recruitment of inflammatory cells, which
61 are in turn infected and used to disseminate throughout the host where they convert into
62 long-lived tissue cysts [4, 5]. Occasionally, cysts reactivate and the released parasites
63 will revert to tachyzoites, which replicate by a unique process termed endodyogeny where
64 the two daughter parasites develop within the mother [6]. Since parasite replication
65 underlies onset of disease in toxoplasmosis patients, it is critical to study the mechanisms
66 regulating endodyogeny.

67 Formation of the inner membrane complex (IMC) is a critical step in endodyogeny.
68 The IMC is a unique organelle comprised of intermediate-filament like cytoskeletal
69 network and membranous sacs whose outer leaflet anchors the actin-myosin gliding
70 machinery [7-9] whereas the cytoplasmic leaflet is associated with subpellicular
71 microtubules that extend from the apical end of the parasite for most of its length [10, 11].
72 During daughter cell development, the IMC emerges from a structure named the daughter
73 cell scaffold (DCS) that is located apically to the parasite's outer core of its bipartite
74 centrosome [12, 13]. The DCS serves as the docking site for Rab11b-regulated vesicles
75 containing the material needed to form the emerging IMC [14]. Despite its central role in
76 endodyogeny, it is largely unknown what proteins localize to the DCS nor is it understood
77 how the DCS regulates IMC assembly.

78 F-box proteins are a family of proteins defined by the presence of a F-box domain
79 and can be divided into three classes, FbxW, FbxL and FbxO [15] according to the
80 presence or absence of canonical substrate recognition domains [15, 16]. F-box proteins
81 are best known as subunits of the Skp1/Cullin/F-box containing E3 ubiquitin ligase (SCF-
82 E3) complex [17] in which the F-box domain binds Skp1 to recruit itself and/or other
83 substrates for polyubiquitination [17, 18]. Although well studied in fungi, plants, and
84 metazoans, the function of F-box proteins in apicomplexan parasites remains unexplored.
85 Previously, we reported that an O_2-regulated *Toxoplasma* prolyl hydroxylase modifies a
86 proline residue in TgSKP1, which can then be modified by a series of glycosyltransferases
87 [19-21]. TgSKP1 prolyl hydroxylation/glycosylation is predicted to alter F-box protein
88 binding leading to changes in substrate recognition [22].
89 Here, we identify 17 putative F-box proteins in the *Toxoplasma* genome that
90 relative to other organisms represents a significantly streamlined repertoire of F-box
91 proteins [23, 24]. We focused on *Toxoplasma* F-box protein 1 (TgFBXO1) and found that
92 it localizes to the DCS early during endodyogeny and is required for DCS function. Thus,
93 TgFBXO1 represents the first protein identified to be an executor of DCS function.
94

95 **RESULTS**

96 **Identification of TgFBXO1 as an Apicomplexan Conserved F-box Protein**

97 F-box proteins contain an F-box domain of ~50 amino acids that are organized into
98 a triple α-helical bundle that mediates binding to Skp1 [25]. The superfamily consists of
99 3 groups that are classified based on the presence of other protein domains: WD40
100 (FbxW), leucine rich (FbxL) repeats and (FbxO) (other domains). We employed a series
101 of reciprocal BLASTp and hidden Markov searches seeded with 43 F-box sequences from
102 known FBPs, including 7 from crystal structures (Figure S1A) and 37 from two well studied
103 yeast species (Figure S1B), to assemble a list of 17 predicted *Toxoplasma gondii* FBPs
104 (Table 1; Figure S1C). Five are of the FbxW and FbxL classes, while the remainder
105 possess C-terminal domains that are poorly if at all are related to FBPs outside of protists
106 (data not shown). All but TgFBXO10 have clear homologs in *Neospora caninum*, but no
107 more than half of the predicted *Toxoplasma* FBPs are conserved in *Plasmodium* and
108 *Eimeria*, indicative of rapid evolutionary specialization. We prioritized *Toxoplasma* F-box
109 proteins for further study as those that are conserved amongst members of the
110 Apicomplexan phylum, important for parasite fitness, and are abundantly expressed in
111 tachyzoites. A genome-wide CRISPR screen revealed that two of four conserved putative
112 F-box proteins, TgFBXO1 (TgGT1_310930) and TgFBXL3 (TgGT1_313200), are
113 important for *Toxoplasma* fitness [26]. In addition, TgFBXO1 is the most strongly
114 expressed *Toxoplasma* F-box protein throughout the tachyzoite cell cycle
115 (http://toxodb.org/toxo/app/record/gene/TGME49_310930).

116 In a parallel study, we sought to identify TgSKP1 interacting proteins via
117 interactome analysis. Thus, RHΔ tachyzoite extracts were incubated with affinity purified

118 anti-TgSKP1 antisera conjugated to Ssepharose beads under non-denaturing conditions.
119 In addition, anti-FLAG antibodies were used to immunoprecipitate TgSKP1 from a
120 *Toxoplasma* strain in which TgSKP1 contains C-terminal Strep/FLAG epitope tags
121 (TgSKP1^{SF}). The immunoprecipitates were subjected to MS/MS analysis and total
122 peptide counts from 3 technical replicates each of two independent trials were analyzed
123 to identify proteins that were immunoprecipated in both samples types and were not found
124 in immunoprecipates obtained using irrelevant antibodies, or in the untagged strain for
125 the anti-FLAG immunoprecipitation.. As expected, TgSKP1, Cullin-1, as well as E1-
126 ubiquitin activating and E2 ubiquitin conjugating enzymes were identified in the TgSKP1
127 immunoprecipitates (Figure 1A). Besides TgSKP1, the two most abundant in the
128 immunoprecipitates were TgGT1_259880, a novel protein with no known function, and
129 TgFBXO1.

130 To confirm TgFBXO1 interacts with SKP1, we tested whether it interacts with
131 TgSKP1 by placing a C-terminal 3XHA epitope tag onto TgFBXO1 (TgFBXO1^{HA}) via
132 homologous recombination [27]. Western blotting lysates from TgFBXO1^{HA} expressing
133 parasites but not the parental RHΔΔ strain with anti-HA antibodies revealed a single
134 immunoreactive band at ~100 kDa, which is the approximate expected molecular weight
135 of TgFBXO1^{HA} (Figure 1; Input 21% O_2). Next, TgSKP1 was detected by Western blotting
136 TgFBXO1^{HA} immunoprecipitates anti-SKP1 antisera (Figure 1B; IP 21% O_2).

137 Previously, we reported that ^{154}Pro of TgSKP1 is hydroxylated and glycosylated
138 and that these post-translational modifications are predicted to change the conformation
139 of the F-box protein-binding region of TgSKP1 as they do in the social amoeba
140 *Dictyostelium discoideum* when a conserved proline residue in DdSKP1 is similarly

141 modified [22]. An O_2-regulated prolyl hydroxylase modifies ^{154}Pro and under low O_2
142 conditions can be observed by Western blotting as a decrease in the apparent molecular
143 weight of TgSKP1 [19, 20, 28] (Figure 1B; TgSKP1 Input Fractions). To test whether
144 TgSKP1 and TgFBXO1 interactions were O_2-dependent, TgSKP1 levels were compared
145 in TgFBXO1^{HA} immunoprecipitates from parasites grown at either 21% or 0.5% O_2. The
146 data revealed modestly increased levels of TgSKP1/TgFBXO1 interactions at 0.5% O_2
147 (Figure 1B; compare 21% O_2 to 0.5% O_2). Together, these data indicate that TgFBXO1
148 is an evolutionarily conserved F-Box protein.
149

150 **TgFBXO1 is Important for Parasite Growth**

151 Attempts to knockout TgFBXO1 by either CRISPR or insertional mutagenesis were
152 unsuccessful suggesting its essentiality (not shown), which is consistent with the finding
153 that it is important for parasite fitness [26]. Similarly, TgFBXO1 was resistant to tagging
154 with the relatively large Destabilization Domain [29]. We therefore used a conditional
155 knockdown system where the TgFBXO1 native promoter was replaced with an
156 anhydrotetracycline (ATC)-repressible promoter and an amino-terminal HA epitope tag
157 was cloned in frame to generate $^{HA(ATC)}$TgFBXO1 (Figure 2A) [30]. $^{HA(ATC)}$TgFBXO1
158 protein was undetectable after 24 h treatment with 1 µg/ml ATC (Figure 2B). Next,
159 $^{HA(ATC)}$TgFBXO1 growth was assessed by plaque assay and significantly fewer plaques
160 were formed by $^{HA(ATC)}$TgFBXO1-depleted parasites (Figure 2C). Moreover, the size of
161 the $^{HA(ATC)}$TgFBXO1 plaques that did form were significantly smaller than the non-
162 depleted plaques (Figure 2D). Because TgFBXO1/TgSKP1 interactions were enhanced
163 at 0.5% O_2, we assessed growth of $^{HA(ATC)}$TgFBXO1 depleted parasites at low O_2 levels.

164 We found that growth of TgFBXO1-depleted parasites was not impacted by O_2 levels
165 (data not shown) and therefore the rest of this study's experiments were performed under
166 normoxic (21% O_2) conditions. Taken together, these data indicate that TgFBXO1 is
167 important for *Toxoplasma* growth.
168

169 **TgFBXO1 Forms an Apical Ring Structure Early During Endodyogeny**

170 While detectable by Western blotting, $^{HA(ATC)}$TgFBXO1 could not be visualized by
171 immunofluorescence staining suggesting inaccessibility of the N-terminal tag in fixed
172 parasites. We therefore assessed TgFBXO1 localization using the C-terminal tagged
173 TgFBXO1^{HA} strain and found that in interphase parasites TgFBXO1 localized to the apical
174 end of the parasite and to the periphery where it colocalized with the IMC protein IMC3,
175 which is a cytoskeletal IMC protein (Figure 3A; G1). We next examined TgFBXO1
176 localization during endodyogeny and found that early during endodyogeny TgFBXO1
177 localized as a ring structure to a perinuclear location before IMC3 formed daughter IMCs
178 (Figure 3A; S-phase). Later during M-phase (note lobe-shaped nuclei that are migrating
179 into nascent daughter cells), TgFBXO1 remained primarily at the apical end of the
180 growing daughter parasites while IMC3 extended posteriorly (Figure 3A; M-phase).

181 ISP1 is another IMC protein that is inserted into the membranous alveoli via fatty
182 acylation. Before IMC3 associates with the daughter IMC, ISP1 forms an apical cap
183 structure in the daughter parasites that remains throughout endodyogeny and into
184 interphase [31]. Comparing ISP1 and TgFBXO1 localization revealed that TgFBXO1
185 associated with its perinuclear localization before ISP1 did (Figure 3B). As parasites
186 progressed through endodyogeny, the ISP1 cap was found near TgFBXO1 although

187 TgFBXO1 was distinct and apical to ISP1 suggesting that the two proteins were distinctly
188 localized within the IMC.

189 We next used a biochemical extraction approach to assess how TgFBXO1
190 associates with the IMC [32]. Parasites were mechanically lysed under hypoosmotic
191 conditions and cytoskeletal fractions were collected by low speed centrifugation. The
192 pellets were resuspended in isotonic buffer and IMC embedded proteins were
193 differentially extracted with salt (electrostatic interaction), Triton X-100 (membrane
194 associated) and SDS (cytoskeletal). TgFBXO1 was extracted with both Triton and SDS
195 indicating that it is most likely associated with the IMC in a manner similar to ISP1 (Figure
196 3C).

197 The first step in endodyogeny is duplication of the parasite's novel bipartite
198 centrosome followed by duplication of the centrocone (a unique nuclear envelop
199 embedded kinetochore), subpellicular microtubule assembly, IMC formation, and finally
200 daughter cell budding and emergence [6, 12, 33]. To more definitively determine when
201 TgFBXO1 apical rings form during endodyogeny, TgFBXO1^{HA} parasites were fixed and
202 stained with anti-Centrin-1 antibodies to detect the centrosomal outer core. We identified
203 parasites where TgFBXO1 remained associated with the mother IMC but containing
204 duplicated centrosomes (Figure 4A; S) indicating that centrosome duplication precedes
205 TgFBXO1 migration. As endodyogeny progressed, TgFBXO1 rings were positioned
206 apically to the duplicated centrosomes (Figure 4A; EM) and as mitosis progressed
207 (denoted by segregating nuclei), centrosomes were associated with medial segments of
208 TgFBXO1 rings (Figure 4A; LM).

209 *Toxoplasma* genome duplication and daughter cell development are coordinated
210 by the parasite MAP kinase, TgMAPK-L1, and in the absence of TgMAPK-L1 signaling
211 centrosome duplication continues although IMC development cannot [30]. We therefore
212 tested whether TgFBXO1 rings formed independently of centrosome duplication by
213 treating TgFBXO1^{HA} parasites with either DMSO (vehicle control) or the TgMAPK-L1
214 inhibitor, SB505124 [34]. In contrast to control parasites, TgFBXO1 staining remained
215 peripheral and daughter apical rings were undetected in SB505124-treated parasites with
216 ≥2 centrosomes (Figure 4B).

217 The *Toxoplasma* centrocone duplicates and separates after centrosome
218 duplication but before ISP and IMC proteins form the daughter cell bud [30, 35]. We
219 therefore compared TgFBXO1 ring formation and centrocone duplication/migration by
220 staining TgFBXO1^{HA} cells with antibodies against the centrocone protein TgNuf2 [36].
221 We identified parasites with distinct TgFBXO1 apical rings that contained duplicated
222 centrocones (note the lobed appearance of TgNuf2 structures) that had not yet separated
223 (Figure 4C; S).

224 Subpellicular microtubules, which provide positional and structural cues for
225 daughter cell IMC development and organization [11], form after centrosome duplication
226 and centrocone separation [37, 38]. To assess the relationship between the TgFBXO1
227 apical rings and daughter cell microtubules, TgFBXO1^{HA} cells were stained with
228 antibodies against acetylated tubulin, which is present stable microtubule filaments [39].
229 Parasites were identified that contained TgFBXO1 apical rings but before acetylated
230 tubulin could be detected in the daughter cells (Figure 5A). As cell cycle progressed,

231 acetylated tubulin colocalized with TgFBXO1 apical rings although F-box protein staining
232 was consistently more apical.

233 To test whether TgFBXO1 apical ring formation was dependent on microtubule
234 assembly, TgFBXO1^{HA} parasites were treated with either DMSO or oryzalin (2.5 μM),
235 which blocks polymerization of parasite but not host microtubules [38]. Oryzalin
236 treatment, which caused the expected defects in microtubule assembly and cytokinesis
237 [40] also led to an accumulation of TgFBXO1 rings with most parasites possessing 8 rings
238 (Figure 5B&C), indicating that the rings formed independently of microtubules.

239

240 **TgFBXO1 Is a Component of the Daughter Cell Scaffold**

241 Collectively, the localization data indicate that TgFBXO1 is recruited to a structure
242 that lies apically to the centrosome outer core and the emerging IMC. The DCS, which
243 serves as a nucleation site for the IMC and microtubules to emerge from, has such a
244 localization [33, 41]. The small molecular weight GTPase TgRab11b localizes early
245 during endodyogeny to the DCS and regulates IMC protein trafficking to the nascent IMC
246 [14]. To compare TgRab11b and TgFBXO1 localization, TgFBXO1^{HA} parasites were
247 transfected with a Rab11b expression construct which contains a C-terminal myc-tagged
248 ddFKBP domain to control protein levels by adding a synthetic ligand, Shield1 [14].
249 Parasites grown in the presence of low Shield1 concentrations (0.1 μM) express low
250 levels of TgRab11b with no apparent affect on growth [14]. Under these conditions,
251 examination of >50 parasites in early S-phase revealed thatTgFBXO1 and TgRab11b co-
252 localized indicating that TgFBXO1 is a DCS component (Figure 6A; top panel). On the
253 other hand, the two proteins did not colocalize in interphase parasites (not shown).

254 To test whether DCS targeting of TgFBXO1 is TgRab11b dependent, TgRab11b-
255 transfected TgFBXO1^{HA} parasites were grown with 1 μM Shield1, which leads to Rab11b
256 dysfunction due to its overexpression [14]. As reported [14], TgRab11b overexpression
257 led to its mislocalization from the DCS and Golgi to the periphery. TgFBXO1 was also
258 mislocalized but unlike TgRab11b appeared as cytoplasmic punctae (Figure 6A).
259 The appearance of TgFBXO1 cytoplasmic punctae in TgRab11b overexpressing
260 parasites suggests that TgFBXO1 traffics to the DCS via membrane trafficking. In
261 addition, TgFBXO1 extractability from the IMC by Triton X-100 (Figure 3C) suggested that
262 like ISP1 it is membrane-associated. TgFBXO1 encodes neither a transmembrane
263 domain nor a signal sequence but contains a consensus N-myristoylation site at ^{2}Gly,
264 which is conserved amongst the coccidian TgFBXO1 homologs (Figure S2). To test
265 whether this potential N-myristoylation site is important for DCS and IMC targeting,
266 parasites were transfected to express either wild-type TgFBXO1 (ptubTgFBXO1^{HA}) or a
267 mutant where ^{2}Gly is mutated to an alanine (ptubTgFBXO1^{HAG2A}). In both interphase and
268 mitotic parasites, ptubTgFBXO1^{HA} was properly localized to the periphery (arrow) and
269 DCS (arrow heads), respectively (Figure 6B). Although ptubTgFBXO1^{HA} overexpression
270 led to enhanced cytoplasmic accumulation of TgFBXO1, this did not impact ISP1
271 localization. In contrast, ptubTgFBXO1^{HAG2A} localization appeared to be largely
272 cytoplasmic and was not localized to either the IMC or DCS. ptubTgFBXO1^{HAG2A}
273 mislocalization had no effect on ISP1 localization indicating that the myristoylation mutant
274 had no dominant negative effect on TgFBXO1 function.
275
276 **TgFBXO1 is Important for DCS Function**

277 To test the importance of TgFBXO1 in DCS function, $^{HA(ATC)}$TgFBXO1 (or parental
278 TATiΔKU80) parasites were grown in the absence or presence of ATC, fixed 24 h later
279 (when TgFBXO1 is undetectable), and stained to detect centrin-1 or ISP1 by
280 immunofluorescence. ATC treatment for 24 h had no effect on ISP1 localization or
281 numbers of parasites (not shown). Since significant growth defects were observed after
282 5 days growth with ATC (Figure 2), these data suggest that low but undetectable amounts
283 of TgFBXO1 protein may be sufficient to support parasite growth.

284 Thus, ISP1 localization was assessed in parasites 5 days after adding ATC.
285 Although ISP1 was localized near centrin-1 in TgFBXO1 depleted parasites, it was
286 disorganized and lacking the typical apical caps found in untreated parasites (Figure 7A).
287 Moreover, the ISP1 cap normally found at the mother cell's apical end was absent in
288 TgFBXO1-depleted parasites.

289 Next, we assessed IMC3 localization and observed that while IMC3 daughter cell
290 buds formed in TgFBXO1-depleted parasites they were often malformed relative to the
291 centrosomes, which presented as several different phenotypes: i) IMC3-labelled daughter
292 buds were associated with nuclei but centrosomes were absent (Figures 7B and S2
293 arrows). ii) Dividing parasites were identified in which only a single IMC was present
294 (Figures 7B and S2 triangles). iii) Nuclei that were devoid of centrosomes and IMC3
295 labeling (Figures 7B and S2 asterisks). Since we cannot determine which specific
296 phenotype is the primary defect, we quantified numbers of parasites with centrosome
297 and/or IMC protein defects and found that ~ 50% of $^{HA(ATC)}$TgFBXO1-depleted parasites
298 displayed a mutant phenotype (Figure 7C). Finally, we also noted some parasites
299 contained IMC3 whirls in mature interphase parasites (Supplemental Figure 2 and Figure

300 7B; **X**), which was reminiscent of the effect of TgRab11b overexpression on IMC3
301 localization [14].

302 Besides development of the IMC, the DCS also promotes assembly of the
303 daughter cell subpellicular microtubules. To examine whether microtubule assembly is
304 affected in TgFBXO1-depleted parasites, $^{HA(ATC)}$TgFBXO1 parasites were grown in the
305 absence or presence of ATC for 5 d and then newly assembled microtubules were imaged
306 using antibodies that recognize acetylated tubulin. In contrast to parasites grown in the
307 absence of ATC, microtubules in the TgFBXO1-depleted parasites were often missing
308 and in others they were not properly organized (Figure 7D). Taken together, these data
309 indicate that TgFBXO1 is a DCS component and is important for IMC maturation and
310 organization during endodyogeny.

311

312

313

314

315 **DISCUSSION**

316 Comprising a ubiquitous eukaryotic protein family, F-box proteins play important
317 roles in diverse biological functions [15, 16]. Although extensively studied in metazoans,
318 plants, and fungi, little is known about their function(s) in protists and in particular
319 Apicomplexans. Here, we identified 17 putative *Toxoplasma* F-box proteins, which
320 approximates the number found in two well studied yeast systems but is considerably
321 less than the number in social amoebae, in humans and other organisms [23, 24].
322 TgFBXO1 was reported to be the most important for parasite fitness [26]; a finding we
323 corroborate using a conditional expression system. We also demonstrated by reciprocal
324 co-immunoprecipitation assays that TgSKP1 and TgFBXO1 interact with each other
325 supporting TgFBXO1 designation as a F-box protein. We further found that TgFBXO1 is
326 a DCS component; a conclusion supported by multiple lines of data. First, it forms a ring-
327 like structure that is positioned apically to the daughter cell centrosome and IMC. Second,
328 TgFBXO1 rings form before ISP1 and IMC3 relocalize to developing daughter parasites.
329 Third, TgFBXO1 relocalization occurs after centrosome duplication but before centrocone
330 separation. Finally, during endodyogeny TgFBXO1 colocalized with Rab11b, the only
331 other known DCS protein, and its DCS localization was Rab11b dependent. We cannot,
332 however, exclude the possibility TgFBXO1 localizes to the recently described
333 pericentriolar matrix [12], which surrounds the centrosome. However, we favor DCS
334 localization since the pericentriolar matrix is thought to be more proximal to the
335 centrosome than the localization reported here for TgFBXO1.

336 Sequence homology-based studies suggest that proteins related to TgFBXO1
337 consist of at least 3 domains (Figure S2). The C-terminal domain and features of the

338 middle predicted F-box domain are conserved in proteins throughout the alveolate clade
339 of protists (Figure S3), which includes ciliates and dinoflagellates as well as
340 apicomplexans. The protein acquired a 330-amino acid N-terminal domain only in
341 *Toxoplasma* and closely related cyst-forming coccidia (no trace of this sequence exists in
342 other extant proteins). Thus, a core function of the FbxO1 clade may have emerged early
343 in evolution to serve an alveolate specific function, such as organization of the
344 membranous villi that lie underneath the plasma membrane, which is the IMC in
345 apicomplexans [42-44].

346 Decreased TgFBXO1 expression had distinct effects on two types of IMC proteins.
347 The IMC alveoli meshwork embedded protein IMC3 formed daughter cell IMCs that were
348 not properly aligned with the centrosome. In contrast, ISP1, which is component of a
349 distinct IMC subcompartment, was unable to form its apical cap structure during
350 endodyogeny and this phenotype was maintained in interphase parasites. While these
351 data are consistent with an emerging model in which IMC components are recruited to
352 the daughter cell through distinct mechanisms [31], they also reveal that the DCS is
353 required for both to occur. It is also possible that only ISP1 or IMC3 require TgFBXO1
354 and that defects observed with the other protein is a downstream effect. Discrimination
355 between these two possibilities awaits characterization of TgFBXO1 interacting proteins.

356 IMC protein trafficking to the DCS and emerging bud is a poorly understood
357 process. The small molecular weight GTPase, Rab11b, is required for this process
358 although it remains unclear where it executes it function and what are its effectors [14].
359 Rab11b and TgFBXO1 both localize to the DCS but their effects on IMC proteins differed
360 – defects in IMC formation vs misaligned daughter buds, respectively. These differences

361 could be due to different approaches to achieving target protein loss of function
362 (overexpression of an inactive Rab11b mutant and TgFBXO1 knockdown) or could
363 represent distinct roles for TgRab11b and TgFBXO1 in IMC biogenesis and organization.
364 But given that TgFBXO1 requires TgRab11b for its DCS localization, we favor a model
365 where TgRab11b functions to recruit diverse types of cargo and membrane vesicles to
366 the DCS and that TgFBXO1 is important for executing DCS function in the development
367 of the new IMC.

368 Using a conditional expression system, TgFBXO1 was found to be required for
369 optimal parasite growth most likely due to its function in regulating IMC development and
370 organization. In initial studies, parasite growth and IMC phenotypes were not evident 24
371 h after adding ATC to $^{HA(ATC)}$TgFBXO1 parasites despite not being able to detect the
372 protein by Western blotting. Rather, the phenotypes were detectable 5 days after adding
373 ATC. One reason for such a delay is that low but undetectable levels of TgFBXO1 are
374 sufficient to sustain replication, a finding previously reported for *Toxoplasma* actin [45].
375 Alternatively, a second F-box protein can compensate for the loss of TgFBXO1 albeit not
376 as efficiently.

377 We are currently unable to differentiate whether TgFBXO1 acts in a SCF-E3
378 ubiquitin ligase dependent or independent manner [15, 46, 47]. It is possible that
379 TgFBXO1 is important for IMC protein ubiquitylation to regulate their turnover and/or
380 targeting during endodyogeny. Such a scenario is supported by the finding that many
381 ubiquitylated *Toxoplasma* proteins are cell cycle regulated including ISP1 and a large
382 number of other IMC proteins [48]. It is also possible that TgFBXO1 is itself an SCF-E3
383 substrate and its ubiquitylation is required during endodyogeny for either trafficking of

384 TgFBXO1 from the IMC to the DCS or for its turnover from the mature IMC early during
385 endodyogeny. It is noteworthy that a parasite deubiquitinase, TgOTUD3 [15, 46, 47, 49,
386 50] was recently reported to coordinate mitosis and cytokinesis by properly matching the
387 correct numbers of centrosomes with numbers of daughter buds. However, we do not
388 believe that TgFBXO1 functions in this manner because in contrast to TgOTUD3, loss of
389 TgFBXO1 leads to unmatched numbers of centrosomes and daughter buds without an
390 increase in parasite ploidy.

391 TgFBXO1 may function in a SCF-E3 ubiquitin ligase independent manner ([51-53].
392 Such a mechanism could occur by the TgSKP1/TgFBXO1 heterodimer, which according
393 to precedent is expected to have high affinity [54-56], being incorporated into a
394 supramolecular complex where TgSKP1 is shielded from interacting with cullin-1 to form
395 a functional SCF complex. Recent cryo-EM studies of the yeast kinetochore provide an
396 example of how the Skp1/Ctf13 (FBP) complex contributes to kinetochore structure in a
397 way where Skp1 is inaccessible to Cul-1 interaction [52, 53]. Certainly, it is conceivable
398 that SCF-E3 dependent or independent mechanisms need not be mutually exclusive,
399 because association with the SCF-E3 could be a mechanism to turn over excess
400 TgFBXO1 that is not associated with the DCS or IMC.

401 In summary, this work represents the first investigation of F-box proteins in
402 Apicomplexan parasites and identify the first DCS-localized protein that is required for
403 DCS function. Identification of TgFBXO1-interacting proteins will allow us to determine
404 how TgFBXO1 executes this function. In addition, it remains to be determined whether
405 TgFBXO1/TgSkp1 interactions are regulated by O_2-dependent hydroxylation and
406 glycosylation of TgSKP1 and whether these impact DCS function or another process.

407

408 **MATERIALS AND METHODS**

409 **F-box Homology Search Methods**

410 Previously, 4 putative F-box-like motifs were identified in the *Toxoplasma* genome
411 based on a hidden Markov algorithm [57]. Further BLASTp [58] studies using F-box-like
412 motifs originating from known F-box domains from 7 crystal structures (Figure S1A), the
413 entire collection of yeast F-box proteins (Figure S1B), and the entire list of F-box-like
414 sequences from *Dictyostelium discoideum* (Figure S1D), and hidden Markov approaches,
415 identified 13 additional putative F-box proteins in *Toxoplasma*. Databases searched
416 included EupathD (https://eupathdb.org/eupathdb/) (*Toxoplasma*, *Neospora caninum*,
417 *Plasmodium* spp, and *Eimeria* spp.), dictyBase (http://dictybase.org/) (*Dictyostelium*),
418 *Saccharomyces* Genome Database (https://www.yeastgenome.org), and PomBase
419 (https://www.pombase.org) (*Schizosaccharomyces*). Each candidate was used to re-
420 search the genome until a comprehensive candidate list was created, which was trimmed
421 of sequences that exceeded the range of variation at individual positions of known F-box
422 sequences (see Figures S1A and S1B) with greatest emphasis given to the pattern of
423 hydrophobic residues. Domain identities were searched using Conserved Domains and
424 Protein Classification search (http://www.ncbi.nlm.nih.gov/Structure/cdd/cdd.shtml)
425 based on database CDDV3.05-42589 PSSMs with E<0.1 (ref. I). Searches were also
426 performed at Uniprot (www.uniprot.org/).

427

428 **Cell Lines and *Toxoplasma* Strains**

429 All parasite strains, including parental RHΔ, TATi-RHΔ*ku80* [59] and RHΔ*ku80*
430 (RHΔΔ) strains [60], were maintained in human foreskin fibroblasts (ATCC; Manassas,

431 VA) in Dulbecco's Modification of Eagle's Medium (DMEM) (VWR; Radnor, PA)
432 supplemented with 10% fetal bovine serum (VWR), 2 mM L-glutamine (VWR), and 100
433 IU/ml penicillin – 100 µg/ml streptomycin (VWR). Parasites were released from host cells
434 by passage through a 27-gauge needle [61]. All parasite strains and host cell lines were
435 routinely tested for Mycoplasma contamination with the MycoAlert Mycoplasma Detection
436 Kit (Lonza, Basel, Switzerland) and found to be negative.
437
438 **Endogenous Epitope Tagging.**
439 The $^{HA(ATC)}$TgFBXO1 conditional expression mutant containing an N-terminal 2x-
440 HA tag was generated by amplifying the 5' end of TgFBXO1 using the following primers
441 (regions of homology to TgFBXO1 are underlined) 5`-
442 GCCAGATCTATGGGCAACACGGAATCC-3` and 5`
443 GCCGCGGCCGCCGATTGATTTTCATGAACCAGTGTG 3`, digested with BglII/NotI and
444 ligated to replace the CEP250 cassette in ptetO7sag4-HA-CEP250-DHFR-TS [30]. The
445 resulting construct was linearized, transfected into the TATiΔku80 strain [30, 59], and
446 clones isolated by limiting dilution using pyrimethamine resistance.
447 TgFBXO1^{HA}, containing a C-terminal 3X-HA tag, was generating by PCR
448 amplifying the 3' region of TgFBXO1 using primers 5'-
449 TACTTCCAATCCAATTTAGCTGAAGCAAGTCCCGAAAGAT 3` AND 5'-
450 TCCTCCACTTCCAATTTTAGCCGCATTGGCTCCGCCCT 3` and incorporated into
451 plasmid pLIC-HA3X-HXGPRT via ligation independent cloning [60]. The construct was
452 linearized and transfected into RHΔku80 strain by electroporation and clones isolated by
453 limiting dilution using mycophenolic acid/xanthine resistance.

454 ptubTgFBXO1^{HA} was generated by synthesizing TgFBXO1 coding sequence
455 (GenScript, Piscataway, NJ) ligating it into p5RT70DDmycRab11b-HXGPRT [14] to
456 replace the DDmycRab11b cassette. Mutation of glycine at position 2 to alanine was
457 accomplished using the Quick Change Mutagenesis kit (Agilent, Santa Clara, CA) to
458 generate ptubTgFBXO1^{HAG2A}.
459

460 **TgSkp1 Interactome Studies**

461 Freshly harvested RHΔΔ or TgSKP1^{SF} [20] tachyzoites (6 × 10^8) were lysed in 1%
462 (v/v) NP-40 in 50 mM HEPES-NaOH (pH 7.4) with protease inhibitors (1 mM PMSF, 10
463 µg/ml aprotinin and 10 µg/ml leupeptin) at 4°C for 10', and then centrifuged at 21,000 x*g*
464 for 15'. The supernatant was precleared with rabbit IgG beads for 60' at 4°C, and Skp1
465 was immunoprecipitated either from RHΔΔ using anti-Skp1 (affinity-purified pAb UOK75)-
466 bound beads (or rabbit IgG-bound beads), or from TgSKP1^{SF} suing anti-FLAG (mAb M2)-
467 bound beads (untagged RHΔΔ lysates were used as a control), that were prepared and
468 used as described [28]. Material was eluted from UOK75 (or control rabbit IgG) beads
469 using 133 mM triethylamine (pH 11.5) for 10' and immediately neutralized with 200 mM
470 acetic acid. mAb M2-bound beads were eluted with 8 M urea in 25 mM NH_4HCO_3 for 15'
471 at 22°C. Eluted samples were denatured with urea, reduced with TCEP, alkylated with
472 iodoacetamide, and trypsinized, and the resulting peptides were analyzed on an Orbitrap
473 Mass Spectrometer (Therme Fisher) as previously described [28]. Only proteins that met
474 the following criteria were reported: i) detected in both types of lysates at a 1% false
475 discovery rate for both peptide and proteins, ii) detected in all 3 technical replicates of two
476 independent samples, iii) not detected in untagged RHΔΔ (TgSKP1^{SF}) or rabbit IgG

477 (UOK75) samples, and iv) were not rhoptry proteins, are reported. Normalized spectral
478 counts and PSMs for protein IDs (1% false discovery rate at both peptide and protein
479 levels) were summed.

480

481 **Plaque Assays**

482 One hundred parasites were added to each well of a 6 well plate containing
483 confluent HFFs in the presence or absence of 1µg/ml ATC. After 5 days, monolayers
484 were methanol-fixed, stained with 0.1% crystal violet, and counted as described [62].

485

486 **Immunoprecipitation**

487 TgFBXO1^{HA} tachyzoites grown at 21% or 0.5% O_2 (in a Baker Hypoxia Chamber
488 (Sanford, ME) were harvested by syringe lysis and washed in ice-cold PBS. Parasites
489 ($1*10^8$) were resuspended in 50 mM Tris-HCl pH 7.4 with 1% Triton X-100, 100 mM NaCl,
490 1 mM NaF, 0.5 mM EDTA, 0.2 mM Na_3VO_4, 1X protease inhibitor cocktail (Thermo Fisher
491 Scientific), incubated on ice for 30 min and then subjected to sonication. Lysates were
492 clarified by centrifugation at 16,000 *x*g, incubated with mouse α-anti-HA clone 12CA5
493 conjugated with protein G beads (Sigma-Aldrich) for 16 hours at 4°C. Immune complexes
494 were separated with SDS-PAGE and then Western blotted with antibodies against rat
495 anti-HA clone 3F10 (Roche) or rabbit anti-TgSkp1 UOK75 [19].

496

497 **IMC Fractionation**

498 IMC fractionation was done essentially as described in [32]. Briefly, freshly
499 harvested tachyzoites were resuspended in hypotonic lysis buffer (10 mM Tris HCl pH

500 7.8, 5 mM NaCl) and lysed by repeated freeze thawing followed by centrifugation at 1,000
501 x*g* to generate fractions S1 (supernatant) and P1 (IMC). S1 was collected and centrifuged
502 at 100,000 x*g* and fractions S2 (cytosol) and P2 (non-IMC membrane) were collected.
503 Fraction P1 was resuspended in isotonic buffer (10 mM Tris HCl pH 7.8, 150 mM NaCl)
504 and centrifuged at 100,000 x*g* for 1 h to isolate proteins that interact with the IMC via
505 electrostatic interactions. Alternatively, SDS or Triton X-100 in isotonic buffer were added
506 to P1 to final concentration of 1% and then centrifuged at 16,000 x*g*. All manipulations
507 were performed at 4ºC and all buffers were supplemented with 1X Protease Inhibitor
508 cocktail.
509

510 **SB505124 and oryzalin treatment**

511 *T. gondii* tachyzoites were allowed to infect HFF monolayers on cover slides for 2
512 hours. Then, parasites were incubated either with 3 μM of SB505124 or equivalent
513 volume of DMSO as a control. After 24 hours, parasites were fixed and analyzed by
514 immunofluorescence. For microtubules disruption, HFF monolayers infected with
515 tachyzoites were incubated with media containing 2.5 μM oryzalin (Sigma). Parasites
516 were allowed to grow 24 hours and then fixed and examined by immunofluorescence.

517

518 **Immunofluorescence Microscopy**

519 *Toxoplasma*-infected HFFs grown on coverslips were fixed either with 4% w/v
520 paraformaldehyde in phosphate buffered saline (PBS) for 20 min at room temperature or
521 by ice-cold methanol for 15 min. Cells were permeabilized with 0.1% Triton X-100 in PBS
522 for 10 min, blocked in 5% w/v bovine serum albumin (BSA) in PBS for 60 min, incubated

523 overnight with primary antibodies at 4ºC, and then incubated for 60 min with Alexa Fluor
524 488- or Alexa Fluor 594-conjugated antibodies (1:2000, Thermo Fisher Scientific).
525 Coverslips were then washed and mounted in DAPI-containing mounting medium (Vector
526 Labs; Burlingame, CA). Images were acquired using a 100X Plan Apo oil immersion 1.46
527 numerical aperture lens on a motorized Zeiss Axioimager M2 microscope equipped with
528 an Orca ER charge-coupled-device (CCD) camera (Hamamatsu, Bridgewater, NJ).
529 Images were collected as a 0.2-μm z-increment serial image stacks, processed using the
530 Volocity, version 6.1, Acquisition Module (Improvision Inc., Lexington, MA). Images were
531 deconvolved by a constrained iterative algorithm, pseudo colored, and merged using the
532 Volocity Restoration Module. All images presented here are maximal projection images
533 and were processed similarly.
534
535

536 **ACKNOWLEDGEMENTS**

537 We would like to thank Drs. Peter Bradley, Vern Carruthers, Marc Jan Gubbels, Markus
538 Meissner, and Elena Suvorova for providing reagents and/or valuable discussion, Kazi
539 Rahman for assistance in predicting F-box domains, and Peng Zhao, Lance Wells, and
540 Steve Hartson for assistance with the proteomic studies.

541

542 **REFERENCES**

543

544 1. Guo M, Mishra A, Buchanan RL, Dubey JP, Hill DE, Gamble HR, et al. A
545 Systematic Meta-Analysis of Toxoplasma gondii Prevalence in Food Animals in the
546 United States. Foodborne Pathog Dis. 2016;13(3):109-18. doi: 10.1089/fpd.2015.2070.
547 PubMed PMID: 26854596;

548 2. Pappas G, Roussos N, Falagas ME. Toxoplasmosis snapshots: global status of
549 Toxoplasma gondii seroprevalence and implications for pregnancy and congenital
550 toxoplasmosis. Int J Parasitol. 2009;39(12):1385-94. Epub 2009/05/13. doi:
551 10.1016/j.ijpara.2009.04.003. PubMed PMID: 19433092;

552 3. Dubey JP. History of the discovery of the life cycle of Toxoplasma gondii. Int J
553 Parasitol. 2009;39(8):877-82. Epub 2009/07/25. PubMed PMID: 19630138;

554 4. Bierly AL, Shufesky WJ, Sukhumavasi W, Morelli AE, Denkers EY. Dendritic cells
555 expressing plasmacytoid marker PDCA-1 are Trojan horses during Toxoplasma gondii
556 infection. J Immunol. 2008;181(12):8485-91. Epub 2008/12/04. doi: 181/12/8485 [pii].
557 PubMed PMID: 19050266;

558 5. Weiss LM, Kim K. The development and biology of bradyzoites of Toxoplasma
559 gondii. Front Biosci. 2000;5:D391-405. PubMed PMID: 10762601;

560 6. Sheffield HG, Melton ML. The fine structure and reproduction of Toxoplasma
561 gondii. J Parasitol. 1968;54(2):209-26. PubMed PMID: 5647101;

562 7. Carruthers V, Boothroyd JC. Pulling together: an integrated model of Toxoplasma
563 cell invasion. Curr Opin Microbiol. 2007;10(1):83-9. Epub 2006/07/14. doi: S1369-
564 5274(06)00100-7 [pii] 10.1016/j.mib.2006.06.017. PubMed PMID: 16837236;

565 8. Russell DG, Sinden RE. Three-dimensional study of the intact cytoskeleton of
566 coccidian sporozoites. Int J Parasitol. 1982;12(2-3):221-6. PubMed PMID: 7076393;

567 9. Mann T, Beckers C. Characterization of the subpellicular network, a filamentous
568 membrane skeletal component in the parasite Toxoplasma gondii. Mol Biochem Parasitol.
569 2001;115(2):257-68. PubMed PMID: 11420112;

570 10. Mann T, Gaskins E, Beckers C. Proteolytic processing of TgIMC1 during
571 maturation of the membrane skeleton of Toxoplasma gondii. J Biol Chem.
572 2002;277(43):41240-6. PubMed PMID: 12177058;

573 11. Morrissette NS, Murray JM, Roos DS. Subpellicular microtubules associate with
574 an intramembranous particle lattice in the protozoan parasite Toxoplasma gondii. J Cell
575 Sci. 1997;110(Pt 1):35-42. PubMed PMID: 9010782;

576 12. Suvorova ES, Francia M, Striepen B, White MW. A novel bipartite centrosome
577 coordinates the apicomplexan cell cycle. PLoS Biol. 2015;13(3):e1002093. doi:
578 10.1371/journal.pbio.1002093. PubMed PMID: 25734885;

579 13. Francia ME, Striepen B. Cell division in apicomplexan parasites. Nat Rev
580 Microbiol. 2014;12(2):125-36. doi: 10.1038/nrmicro3184. PubMed PMID: 24384598;

581 14. Agop-Nersesian C, Egarter S, Langsley G, Foth BJ, Ferguson DJ, Meissner M.
582 Biogenesis of the inner membrane complex is dependent on vesicular transport by the
583 alveolate specific GTPase Rab11B. PLoS Pathog. 2010;6(7):e1001029. doi:
584 10.1371/journal.ppat.1001029. PubMed PMID: 20686666;

585 15. Nelson DE, Randle SJ, Laman H. Beyond ubiquitination: the atypical functions of
586 Fbxo7 and other F-box proteins. Open Biol. 2013;3(10):130131. doi:
587 10.1098/rsob.130131. PubMed PMID: 24107298;

588 16. Wang Z, Liu P, Inuzuka H, Wei W. Roles of F-box proteins in cancer. Nat Rev
589 Cancer. 2014;14(4):233-47. doi: 10.1038/nrc3700. PubMed PMID: 24658274;

590 17. Bai C, Sen P, Hofmann K, Ma L, Goebl M, Harper JW, et al. SKP1 connects cell
591 cycle regulators to the ubiquitin proteolysis machinery through a novel motif, the F-box.
592 Cell. 1996;86(2):263-74. PubMed PMID: 8706131;

593 18. Skowyra D, Craig KL, Tyers M, Elledge SJ, Harper JW. F-box proteins are
594 receptors that recruit phosphorylated substrates to the SCF ubiquitin-ligase complex.
595 Cell. 1997;91(2):209-19. PubMed PMID: 9346238;

596 19. Xu Y, Brown KM, Wang ZA, van der Wel H, Teygong C, Zhang D, et al. The Skp1
597 protein from Toxoplasma is modified by a cytoplasmic prolyl 4-hydroxylase associated
598 with oxygen sensing in the social amoeba Dictyostelium. J Biol Chem.
599 2012;287(30):25098-110. Epub 2012/06/01. doi: 10.1074/jbc.M112.355446. PubMed
600 PMID: 22648409;

601 20. Rahman K, Mandalasi M, Zhao P, Sheikh MO, Taujale R, Kim HW, et al.
602 Characterization of a cytoplasmic glucosyltransferase that extends the core trisaccharide
603 of the Toxoplasma Skp1 E3 ubiquitin ligase subunit. J Biol Chem. 2017;292(45):18644-
604 59. doi: 10.1074/jbc.M117.809301. PubMed PMID: 28928220;

605 21. Rahman K, Zhao P, Mandalasi M, van der Wel H, Wells L, Blader IJ, et al. The E3-
606 ubiquitin ligase adaptor protein Skp1 is glycosylated by an evolutionarily conserved
607 pathway that regulates protist growth and development. J Biol Chem. 2015;291(9):4268-
608 80. Epub December, 30, 2015. doi: 10.1074/jbc.M115.703751. PubMed PMID:
609 26719340;

610 22. Sheikh MO, Thieker D, Chalmers G, Schafer CM, Ishihara M, Azadi P, et al. O2
611 sensing-associated glycosylation exposes the F-box-combining site of the Dictyostelium
612 Skp1 subunit in E3 ubiquitin ligases. J Biol Chem. 2017;292(46):18897-915. doi:
613 10.1074/jbc.M117.809160. PubMed PMID: 28928219;

614 23. Kipreos ET, Pagano M. The F-box protein family. Genome Biol.
615 2000;1(5):REVIEWS3002. doi: 10.1186/gb-2000-1-5-reviews3002. PubMed PMID:
616 11178263;

617 24. Lechner E, Achard P, Vansiri A, Potuschak T, Genschik P. F-box proteins
618 everywhere. Curr Opin Plant Biol. 2006;9(6):631-8. doi: 10.1016/j.pbi.2006.09.003.
619 PubMed PMID: 17005440;

620 25. Schulman BA, Carrano AC, Jeffrey PD, Bowen Z, Kinnucan ERE, Finnin MS, et al.
621 Insights into SCF ubiquitin ligases from the structure of the Skp1–Skp2 complex. Nature.
622 2000;408:381. doi: 10.1038/35042620. PubMed PMID: 11099048;

623 26. Sidik SM, Huet D, Ganesan SM, Huynh MH, Wang T, Nasamu AS, et al. A
624 Genome-wide CRISPR Screen in Toxoplasma Identifies Essential Apicomplexan Genes.
625 Cell. 2016;166(6):1423-35 e12. doi: 10.1016/j.cell.2016.08.019. PubMed PMID:
626 27594426;

627 27. Fox BA, Ristuccia JG, Gigley JP, Bzik DJ. Efficient gene replacements in
628 Toxoplasma gondii strains deficient for nonhomologous end joining. Eukaryot Cell.
629 2009;8(4):520-9. PubMed PMID: 19218423;

630 28. Sheikh MO, Xu Y, van der Wel H, Walden P, Hartson SD, West CM. Glycosylation
631 of Skp1 promotes formation of Skp1-cullin-1-F-box protein complexes in dictyostelium.
632 Mol Cell Proteomics. 2015;14(1):66-80. doi: 10.1074/mcp.M114.044560. PubMed PMID:
633 25341530;

634 29. Armstrong CM, Goldberg DE. An FKBP destabilization domain modulates protein
635 levels in Plasmodium falciparum. Nat Methods. 2007;4(12):1007-9. PubMed PMID:
636 17994030;

637 30. Alvarez CA, Suvorova ES. Checkpoints of apicomplexan cell division identified in
638 Toxoplasma gondii. PLoS Pathog. 2017;13(7):e1006483. doi:
639 10.1371/journal.ppat.1006483. PubMed PMID: 28671988;

640 31. Beck JR, Rodriguez-Fernandez IA, Cruz de Leon J, Huynh MH, Carruthers VB,
641 Morrissette NS, et al. A novel family of Toxoplasma IMC proteins displays a hierarchical
642 organization and functions in coordinating parasite division. PLoS Pathog.
643 2010;6(9):e1001094. Epub 2010/09/17. doi: 10.1371/journal.ppat.1001094. PubMed
644 PMID: 20844581;

645 32. Dubey R, Staker BL, Foe IT, Bogyo M, Myler PJ, Ngo HM, et al. Membrane skeletal
646 association and post-translational allosteric regulation of Toxoplasma gondii GAPDH1.
647 Mol Microbiol. 2017;103(4):618-34. Epub 2016/11/20. doi: 10.1111/mmi.13577. PubMed
648 PMID: 27859784;

649 33. Nishi M, Hu K, Murray JM, Roos DS. Organellar dynamics during the cell cycle of
650 Toxoplasma gondii. J Cell Sci. 2008;121(Pt 9):1559-68. Epub 2008/04/16. doi:
651 10.1242/jcs.021089. PubMed PMID: 18411248;

652 34. Brown KM, Suvorova E, Farrell A, McLain A, Dittmar A, Wiley GB, et al. Forward
653 genetic screening identifies a small molecule that blocks Toxoplasma gondii growth by
654 inhibiting both host- and parasite-encoded kinases. PLoS Pathog. 2014;10(6):e1004180.
655 Epub 2014/06/20. doi: 10.1371/journal.ppat.1004180. PubMed PMID: 24945800;

656 35. Gubbels MJ, Vaishnava S, Boot N, Dubremetz JF, Striepen B. A MORN-repeat
657 protein is a dynamic component of the Toxoplasma gondii cell division apparatus. J Cell
658 Sci. 2006;119(Pt 11):2236-45. Epub 2006/05/11. doi: jcs.02949 [pii] 10.1242/jcs.02949.
659 PubMed PMID: 16684814;

660 36. Farrell M, Gubbels M-J. The Toxoplasma gondii kinetochore is required for
661 centrosome association with the centrocone (spindle pole). Cellular Microbiology.
662 2013;16(1):78-94. doi: 10.1111/cmi.12185. PubMed PMID: 24015880;

663 37. Shaw MK, Compton HL, Roos DS, Tilney LG. Microtubules, but not actin filaments,
664 drive daughter cell budding and cell division in Toxoplasma gondii. J Cell Sci. 2000;113 (
665 Pt 7):1241-54. Epub 2000/03/08. PubMed PMID: 10704375;

666 38. Morrissette NS, Sibley LD. Disruption of microtubules uncouples budding and
667 nuclear division in Toxoplasma gondii. J Cell Sci. 2002;115(Pt 5):1017-25. Epub
668 2002/03/01. PubMed PMID: 11870220;

669 39. Westermann S, Weber K. Post-translational modifications regulate microtubule
670 function. Nat Rev Mol Cell Biol. 2003;4(12):938-47. doi: 10.1038/nrm1260. PubMed
671 PMID: 14685172;

672 40. Morrissette NS, Mitra A, Sept D, Sibley LD. Dinitroanilines bind alpha-tubulin to
673 disrupt microtubules. Mol Biol Cell. 2004;15(4):1960-8. Epub 2004/01/27. doi:
674 10.1091/mbc.E03-07-0530 PubMed PMID: 14742718;

675 41. Blader IJ, Coleman BI, Chen CT, Gubbels MJ. Lytic Cycle of Toxoplasma gondii:
676 15 Years Later. Annu Rev Microbiol. 2015;69:463-85. doi: 10.1146/annurev-micro-
677 091014-104100. PubMed PMID: 26332089;

678 42. Kono M, Herrmann S, Loughran NB, Cabrera A, Engelberg K, Lehmann C, et al.
679 Evolution and architecture of the inner membrane complex in asexual and sexual stages

680 of the malaria parasite. Mol Biol Evol. 2012;29(9):2113-32. Epub 2012/03/06. doi:
681 10.1093/molbev/mss081. PubMed PMID: 22389454;

682 43. Morrissette NS, Sibley LD. Cytoskeleton of apicomplexan parasites. Microbiol Mol
683 Biol Rev. 2002;66(1):21-38; table of contents. Epub 2002/03/05. PubMed PMID:
684 11875126;

685 44. Lee RE, Kugrens P. Relationship between the flagellates and the ciliates. Microbiol
686 Rev. 1992;56(4):529-42. Epub 1992/12/01. PubMed PMID: 1480107;

687 45. Drewry LL, Sibley LD. Toxoplasma Actin Is Required for Efficient Host Cell
688 Invasion. MBio. 2015;6(3):e00557. doi: 10.1128/mBio.00557-15. PubMed PMID:
689 26081631;

690 46. Peng D, Wang Z, Huang A, Zhao Y, Qin FX. A Novel Function of F-Box Protein
691 FBXO17 in Negative Regulation of Type I IFN Signaling by Recruiting PP2A for IFN
692 Regulatory Factor 3 Deactivation. J Immunol. 2017;198(2):808-19. doi:
693 10.4049/jimmunol.1601009. PubMed PMID: 27956528;

694 47. Smaldone S, Laub F, Else C, Dragomir C, Ramirez F. Identification of MoKA, a
695 novel F-box protein that modulates Kruppel-like transcription factor 7 activity. Mol Cell
696 Biol. 2004;24(3):1058-69. PubMed PMID: 14729953;

697 48. Silmon de Monerri NC, Yakubu RR, Chen AL, Bradley PJ, Nieves E, Weiss LM, et
698 al. The Ubiquitin Proteome of Toxoplasma gondii Reveals Roles for Protein Ubiquitination
699 in Cell-Cycle Transitions. Cell Host Microbe. 2015;18(5):621-33. doi:
700 10.1016/j.chom.2015.10.014. PubMed PMID: 26567513;

701 49. Dhara A, de Paula Baptista R, Kissinger JC, Snow EC, Sinai AP. Ablation of an
702 Ovarian Tumor Family Deubiquitinase Exposes the Underlying Regulation Governing the
703 Plasticity of Cell Cycle Progression in Toxoplasma gondii. MBio. 2017;8(6). doi:
704 10.1128/mBio.01846-17. PubMed PMID: 29162714;

705 50. Liu Y, Nakatsukasa K, Kotera M, Kanada A, Nishimura T, Kishi T, et al. Non-SCF-
706 type F-box protein Roy1/Ymr258c interacts with a Rab5-like GTPase Ypt52 and inhibits
707 Ypt52 function. Mol Biol Cell. 2011;22(9):1575-84. Epub 2011/03/11. doi:
708 10.1091/mbc.E10-08-0716. PubMed PMID: 21389113;

709 51. Hermand D. F-box proteins: more than baits for the SCF? Cell Div. 2006;1:30.
710 Epub 2006/12/15. doi: 10.1186/1747-1028-1-30. PubMed PMID: 17166256;

711 52. Zhang W, Lukoynova N, Miah S, Lucas J, Vaughan CK. Insights into Centromere
712 DNA Bending Revealed by the Cryo-EM Structure of the Core Centromere Binding Factor
713 3 with Ndc10. Cell Rep. 2018;24(3):744-54. Epub 2018/07/19. doi:
714 10.1016/j.celrep.2018.06.068. PubMed PMID: 30021170;

715 53. Leber V, Nans A, Singleton MR. Structural basis for assembly of the CBF3
716 kinetochore complex. EMBO J. 2018;37(2):269-81. Epub 2017/12/08. doi:
717 10.15252/embj.201798134. PubMed PMID: 29212814;

718 54. Li T, Pavletich NP, Schulman BA, Zheng N. High-level expression and purification
719 of recombinant SCF ubiquitin ligases. Methods Enzymol. 2005;398:125-42. Epub
720 2005/11/09. doi: 10.1016/S0076-6879(05)98012-9. PubMed PMID: 16275325;

721 55. van der Wel H, Johnson JM, Xu Y, Karunaratne CV, Wilson KD, Vohra Y, et al.
722 Requirements for Skp1 processing by cytosolic prolyl 4(trans)-hydroxylase and alpha-N-
723 acetylglucosaminyltransferase enzymes involved in O(2) signaling in dictyostelium.
724 Biochemistry. 2011;50(10):1700-13. Epub 2011/01/21. doi: 10.1021/bi101977w. PubMed
725 PMID: 21247092;

726 56. Tan A, Tanner JJ, Henzl MT. Energetics of OCP1-OCP2 complex formation.
727 Biophys Chem. 2008;134(1-2):64-71. Epub 2008/02/21. doi: 10.1016/j.bpc.2008.01.005.
728 PubMed PMID: 18284940;

729 57. Ponts N, Yang J, Chung DW, Prudhomme J, Girke T, Horrocks P, et al.
730 Deciphering the ubiquitin-mediated pathway in apicomplexan parasites: a potential
731 strategy to interfere with parasite virulence. PLoS One. 2008;3(6):e2386. Epub
732 2008/06/12. doi: 10.1371/journal.pone.0002386. PubMed PMID: 18545708;

733 58. Altschul SF, Wootton JC, Gertz EM, Agarwala R, Morgulis A, Schaffer AA, et al.
734 Protein database searches using compositionally adjusted substitution matrices. FEBS J.
735 2005;272(20):5101-9. Epub 2005/10/13. doi: 10.1111/j.1742-4658.2005.04945.x.
736 PubMed PMID: 16218944;

737 59. Sheiner L, Demerly JL, Poulsen N, Beatty WL, Lucas O, Behnke MS, et al. A
738 systematic screen to discover and analyze apicoplast proteins identifies a conserved and
739 essential protein import factor. PLoS Pathog. 2011;7(12):e1002392. Epub 2011/12/07.
740 doi: 10.1371/journal.ppat.1002392. PubMed PMID: 22144892;

741 60. Huynh MH, Carruthers VB. Tagging of endogenous genes in a Toxoplasma gondii
742 strain lacking Ku80. Eukaryot Cell. 2009;8(4):530-9. PubMed PMID: 19218426;

743 61. Wiley M, Sweeney KR, Chan DA, Brown KM, McMurtrey C, Howard EW, et al.
744 Toxoplasma gondii activates hypoxia-inducible factor (HIF) by stabilizing the HIF-1alpha
745 subunit via type I activin-like receptor kinase receptor signaling. J Biol Chem.
746 2010;285(35):26852-60. doi: 10.1074/jbc.M110.147041. PubMed PMID: 20581113;

747 62. Spear W, Chan D, Coppens I, Johnson RS, Giaccia A, Blader IJ. The host cell
748 transcription factor hypoxia-inducible factor 1 is required for Toxoplasma gondii growth
749 and survival at physiological oxygen levels. Cell Microbiol. 2006;8(2):339-52. doi:
750 10.1111/j.1462-5822.2005.00628.x. PubMed PMID: 16441443;

751

752

753 **FIGURE LEGENDS**

754

755 **Fig 1. TgFBXO1 Interacts with TgSKP1. (A).** RHΔ and TgSKP1^{SF} tachyzoites were
756 solubilized and immunoprecipitated with affinity purified anti-Tg Skp1 (UOK75) or anti-
757 FLAG (M2) respectively. The immunoprecipitates were trypsin digested and subjected to
758 proteomic analysis. Protein hits are reported as those proteins identified in both samples
759 and for which no spectral counts were recovered in immunoprecipitates obtained with
760 irrelevant antibodies (for UOK75) or the untagged strain (for M2). An additional filter was
761 applied to exclude abundant rhoptry proteins. **(B).** Lysates prepared from TgFBXO1^{HA}
762 and parental RHΔKU80 grown at 21% or 0.5% O_2 were either Western blotted (Input) or
763 incubated with anti-HA antibodies (IP). The immunoprecipitates were captured by Protein
764 G Sepharose and the immune complexes were Western blotted to detect TgFBXO1^{HA},
765 TgSkp1, and SAG1.

766

767 **Figure 2. TgFBXO1 is Important for *Toxoplasma* growth. (A).** Schematic illustration
768 of $^{HA(ATC)}$TgFBXO1 anhydrotetracycline (ATC) mediated gene expression. The TgFBXO1
769 endogenous promoter was replaced with a SAG4 promoter containing a tetracycline
770 transactivator (tTA) binding element. In the absence of ATC, the tetracycline regulated
771 promoter is active, while the addition of ATC reduces transcription by preventing tTA
772 binding to and activating the promoter. **(B).** Lysates from $^{HA(ATC)}$TgFBXO1 or parental
773 TATiΔKU80 parasites grown for 24 h in the absence or presence of 1μg/ml ATC were
774 Western blotted to detect $^{HA(ATC)}$TgFBXO1 or SAG1 as a loading control. **(C).**
775 $^{HA(ATC)}$TgFBXO1 or TATiΔKU80 parasites (100/well of a 6 well plate) were grown for 5 d

776 on HFF monolayers with or without 1μg/ml ATC. The cells were then fixed and numbers
777 of plaques formed counted. Shown are the averages and standard deviations of 3
778 independent experiments performed in triplicate. **(D).** Representative images of plaques
779 from (C) showing decreased plaque size of TgFBXO1-depleted parasites. Plaque sizes
780 were quantified and plotted on the adjacent graph. *, $p < 0.001$, One-Way ANOVA.
781
782 **Figure 3. TgFBXO1 Forms Apical Rings Early During Endodyogeny. (A).**
783 TgFBXO1^{HA}-expressing parasites were fixed and stained to detect IMC3, TgFBXO1, and
784 DNA during G1, S, and M phases. Arrows highlight TgFBXO1 apical rings. **(B).**
785 TgFBXO1^{HA}-expressing parasites were fixed and stained to detect ISP1, TgFBXO1, and
786 DNA during S, early M (before nuclear segregation), and late M (during nuclear
787 segregation) phases. Arrows highlight TgFBXO1 apical rings. Bars = 2μm. **(C).** TOP:
788 Fractionation scheme to characterize TgFBXO1^{HA} association with the IMC. BOTTOM:
789 Western blotting of equivalent volumes of each indicated fraction. Blots were probed with
790 antibodies to detect TgFBXO1 (α-HA), IMC3 (αIMC3), and ISP1 (αISP1).
791
792 **Figure. 4. TgFBXO1 Rings are Localized Apically to the Parasite Centrosome and**
793 **Form After Centrosome Duplication. (A).** TgFBXO1^{HA}-expressing parasites were fixed
794 and stained to detect TgCentrin1, TgFBXO1, and DNA during S, early M (EM), and late
795 M (LM) phases. Arrows highlight TgFBXO1 apical rings. Bars = 2μm. A schematic
796 depicting the cell cycle phases is shown. **(B).** Parasites were treated with 3 μM SB505124
797 (or DMSO as a vehicle control) for 24 h, fixed and then stained to detect TgCentrin1,
798 TgFBXO1, and DNA. Note the appearance of SB505124-treated parasites with >2

799 centrosomes and disorganized TgFBXO1 staining. Bars = 5 μm. **(C).** TgFBXO1^{HA}
800 parasites were stained to detect TgFBXO1 and the centrocone marker TgNuf2. Note
801 TgFBXO1^{HA} apical rings form after centrocone duplication but before separation as
802 evidenced by the lobed TgNuf2 staining (Insert). Bars: 2μm.
803
804 **Figure 5. TgFBXO1 Apical Rings form Independently of Daughter Cell Microtubule**
805 **Assembly. (A).** TgFBXO1^{HA}-expressing parasites were stained to detect TgFBXO1,
806 acetylated tubulin (to detect newly synthesized microtubules), and DNA during S, early
807 M, and late M (during nuclear segregation) phases. **(B).** Parasites were treated with
808 oryzalin (2.5 μM) or DMSO (vehicle control) for 24 h and then stained to detect TgFBXO1,
809 acetylated tubulin, and DNA. Arrowheads highlight TgFBXO1 apical rings. Bars = 2 μm.
810 **(C).** Quantification of numbers of TgFBXO1^{HA} rings per parasite that form in the presence
811 of DMSO or oryzalin. Shown are the averages and standard deviations of 3 independent
812 experiments in which 50 randomly selected parasites per experiment were counted.
813
814 **Figure 6. TgFBXO1 Is Recruited to the DCS in a Rab11b-Dependent Manner. (A).**
815 TgFBXO1^{HA}-expressing parasites were transiently transfected with
816 p5RT70DDmycRab11b-HXGPRT expression construct and then grown in the presence
817 of Shield-1 (0.1μM - low level expression or 1 μM – high level expression) reagent for 48
818 h. Cells were then fixed and stained to detect TgRab11b or TgFBXO1. Arrows highlight
819 apparent colocalization of Rab11b with the TgFBXO1 apical rings. Bars = 2μm. **(B).**
820 Parasites were transiently transfected with wild-type (ptubTgFBXO1^{HA}) or myristoylation
821 mutant (ptubTgFBXO1^{HAG2A}) TgFBXO1 expression constructs, fixed 48 h later, and

822 stained to detect ISP1 and TgFBXO1. Arrows highlight position of IMC1 apical caps.
823 Bars = 2 µm.
824
825 **Figure 7. TgFBXO1 Is Required for IMC Organization and Maturation. (A).** Parental
826 TATiΔku80 and $^{HA(ATC)}$TgFBXO1 parasites were grown in the absence or presence of ATC
827 (1 µg/ml) for 5 days and stained to detect ISP1 and TgCentrin1. * denotes mislocalized
828 ISP1 in DCS of parasites with decreased TgFBXO1 expression. Bars = 1 µm. **(B).**
829 Parental TATiΔku80 and $^{HA(ATC)}$TgFBXO1 parasites were grown in the absence or
830 presence of ATC (1 µg/ml) for 5 days and stained to detect IMC3 and TgCentrin1. ⊕
831 highlights IMC3 whirls, * highlights parasites lacking IMC3 staining, arrows highlight
832 misaligned IMC3 and centrosomes, and arrowheads highlight parasites lacking
833 centrosomes. Bars = 2 µm. **(C).** Quantification of IMC3/centrosome mislocalization in at
834 10 randomly selected fields per condition. Shown are averages and standard deviations
835 of 3 independent experiments.
836
837

838 **SUPPORTING INFORMATION LEGENDS**

839 **Figure S1. Known and Predicted F-box Proteins.** F-box domain sequences were
840 predicted as described in Methods. To facilitate visualization of relatedness, acidic
841 residues are in blue, basic in dark red, small or prolines in red, and hydrophobic in green.
842 Positions matching the consensus motif are highlighted in yellow (hydrophobic), gray
843 (acidic), green (basic), or teal (small). F-box sequences from known structures and other
844 validated studies, and functional and interactome studies in *Schizosaccharomyces*
845 *pombe* and *Saccharomyces cerevisiae*, were aligned to characterize the known diversity
846 of F-box domains. The family of consensus sequences was used to search the genomes
847 of *Toxoplasma*, other apicomplexans, and the social amoeba *Dictyostelium discoideum*.
848 **(A.)** Representative F-box motif sequences derived from crystal structures of F-box
849 protein/Skp1 complexes and other well-known F-box proteins. **(B).** F-box motif
850 sequences from the yeasts *S. pombe* and *S. cerevisiae*. **(C).** Candidate F-box motif
851 sequences from *Toxoplasma gondii* (type 1 strain ME49). **(D).** Predicted F-box motif
852 sequences from *D. discoideum*. FbxO1-like sequences were not detected in the *D.*
853 *discoideum* genome.

854

855 **Figure S2. FBXO1 Evolution.** Sequences homologous to *T. gondii* FbxO1 were aligned
856 in COBALT and subject to manual refinement. To facilitate visualization of relatedness,
857 acidic residues are in blue, basic in dark red, small or prolines in red, and hydrophobic in
858 green. Positions of similarity in one group are highlighted in yellow (hydrophobic), gray
859 (acidic), green (basic), or teal (small). Underlines separate phylogenetic groups: the top
860 two groups consist of different coccidian subclades, the next two groups represent other

861 apicomplexans, the next group contains a chromerid (apicomplexan predecessor), and
862 the bottom group contains non-apicomplexan alveolates including ciliates and
863 dinoflagellates.

864

865 **Figure S3. FbxO1 Domain Prediction.** Sequence-based homology (Figure S2)
866 suggests that Tg-FbxO1 consists of at least 3 domains. **(A).** *T. gondii* FbxO1. Other
867 coccidians conserve this architecture. The N-domain is conserved in length and general
868 amino acid composition, but only the regions shaded in blue, including the N-terminal N-
869 myristylation motif (GxxxS), are conserved in sequence. **(B).** Non-coccidian
870 apicomplexans and other alveolates. The ~370 C-terminal region is generally conserved
871 in all alveolate sequences. This region includes an N-terminally positioned predicted F-
872 box domain (F) and the C-domain. Some alveolate sequences consist of only F- and C-
873 domains, whereas others contain N-terminal extensions of variable length (dashed line)
874 that bear no detectable sequence similarity to the N-domain of TgFBXO1.

875

876 **Supplemental Table S1. *Toxoplasma* F-box Proteins**. Shown are the 17 predicted
877 *Toxoplasma* F-box proteins identified in this study. The ToxoDB or PlasmoDB IDs contain
878 hyperlinks to relevant web pages at the EUPATHDB Genome DatabaseS
879 (www.eupathDB.org). Sidik et al Fitness Scores are from [26].

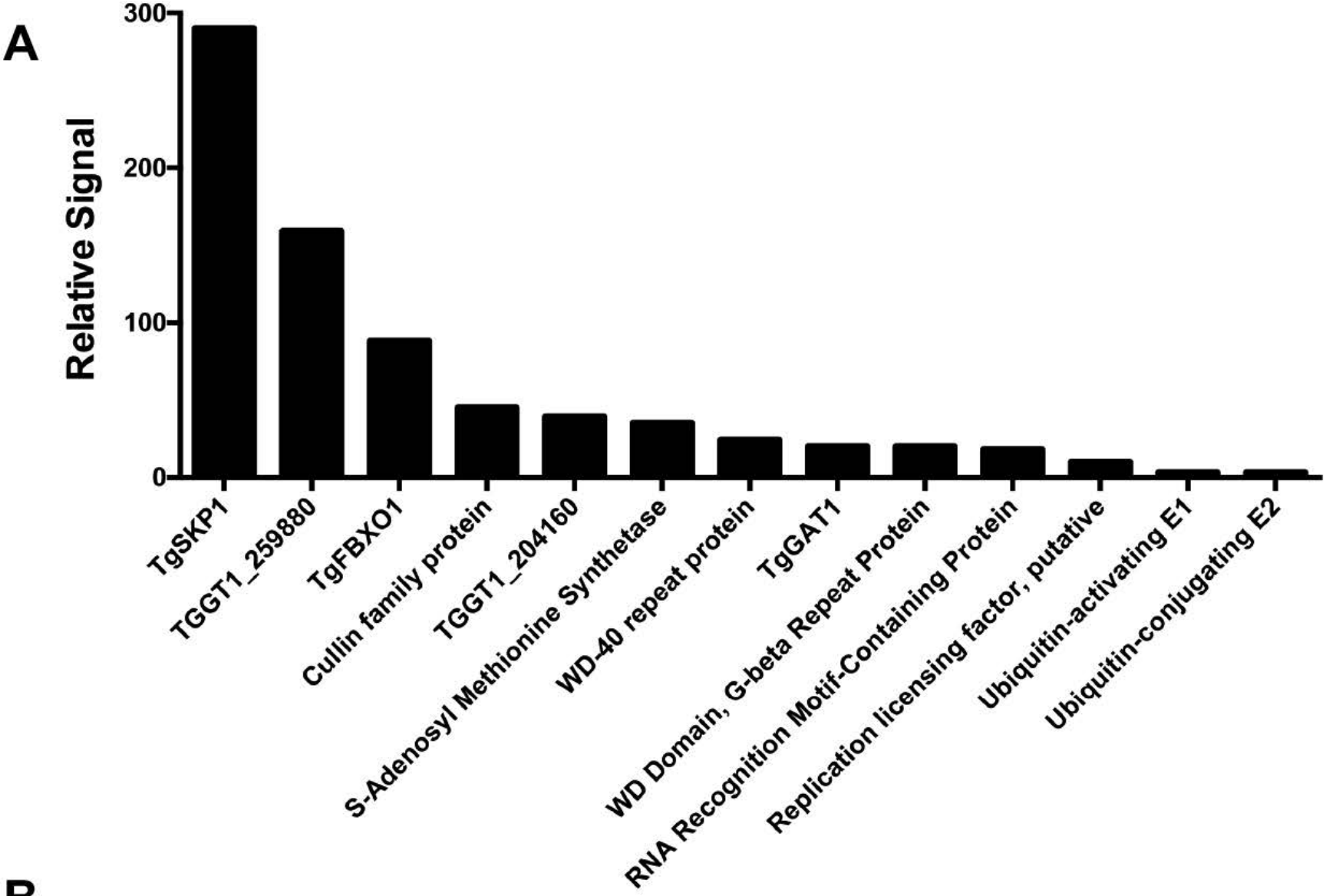
A
Relative Signal
300
200
100
0
TgSKP1
TGGT1_259880
TgFBXO1
Cullin family protein
TGGT1_204160
S-Adenosyl Methionine Synthetase
WD-40 repeat protein
TgGAT1
WD Domain, G-beta Repeat Protein
RNA Recognition Motif-Containing Protein
Replication licensing factor, putative
Ubiquitin-activating E1
Ubiquitin-conjugating E2

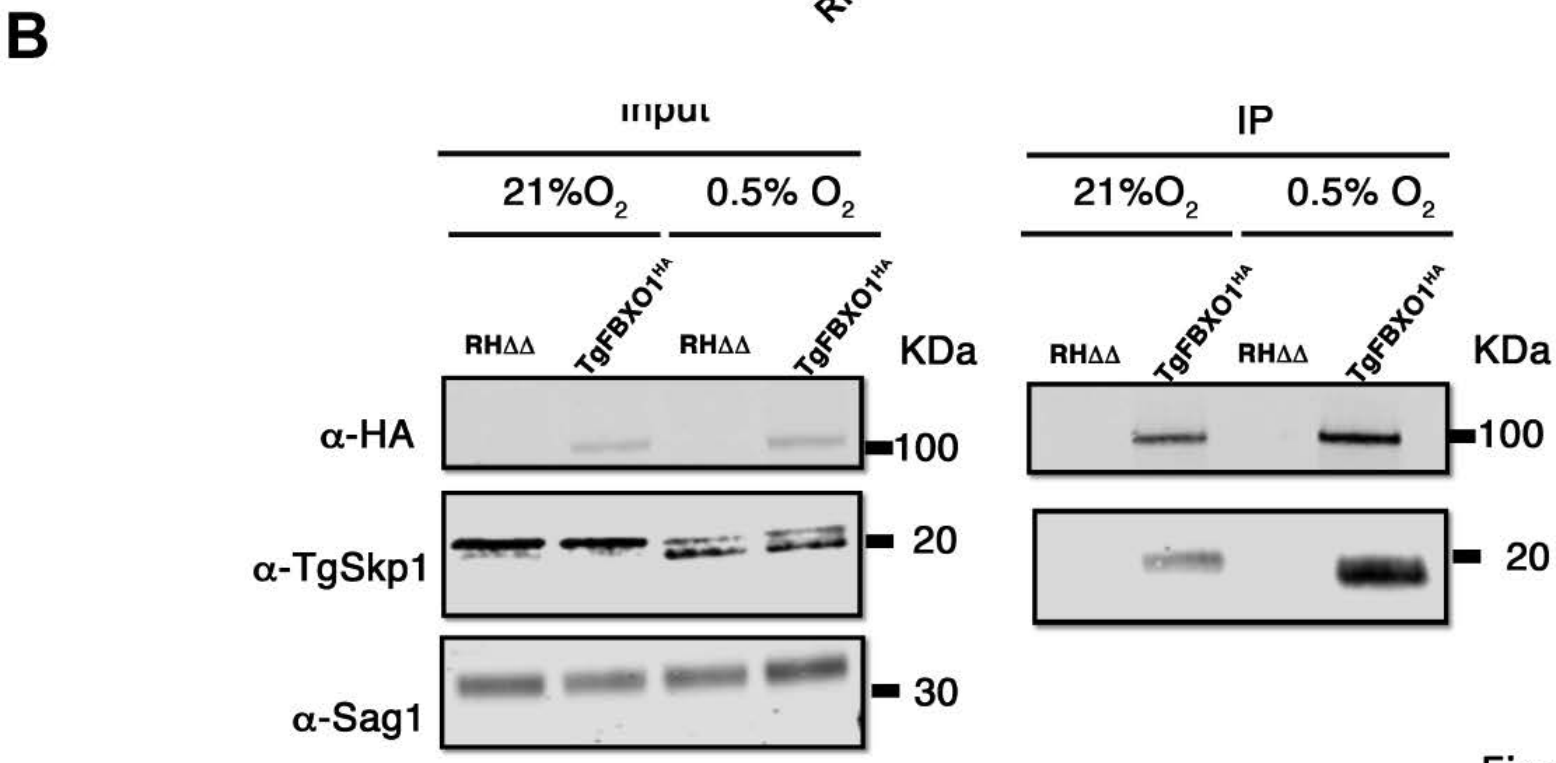
B
Input
IP
21%O2
0.5% O2
21%O2
0.5% O2
RHΔΔ
TgFBXO1HA
RHΔΔ
TgFBXO1HA
KDa
RHΔΔ
TgFBXO1HA
RHΔΔ
TgFBXO1HA
KDa
α-HA
α-TgSkp1
α-Sag1
100
20
30
100
20

Figure 1

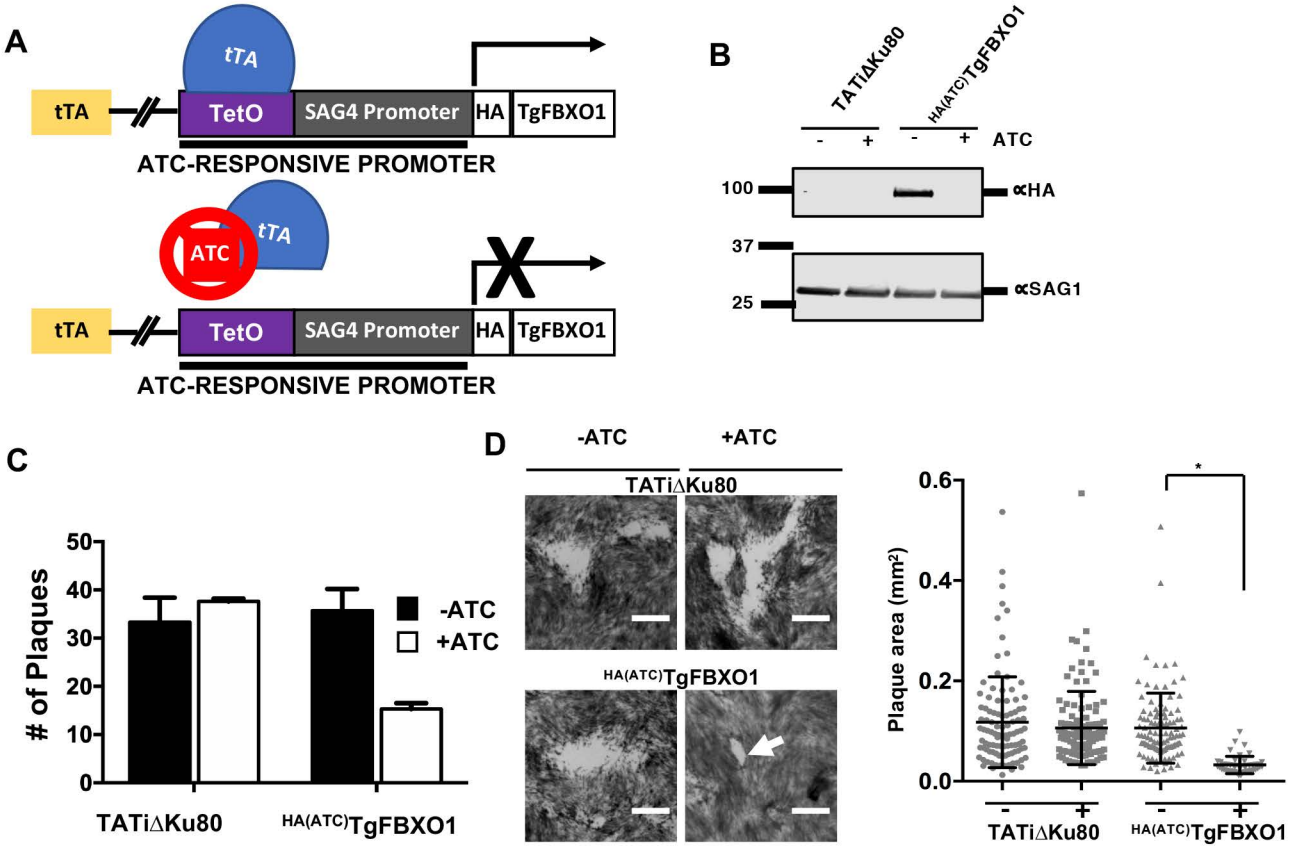
A
tTA
tTA
TetO
SAG4 Promoter
HA
TgFBXO1
ATC-RESPONSIVE PROMOTER
ATC
tTA
tTA
TetO
SAG4 Promoter
HA
TgFBXO1
ATC-RESPONSIVE PROMOTER
B
TATiΔKu80
HA(ATC)TgFBXO1
- + - +
ATC
100
37
25
αHA
αSAG1
C
# of Plaques
50
40
30
20
10
0
-ATC
+ATC
TATiΔKu80
HA(ATC)TgFBXO1
D
-ATC
+ATC
TATiΔKu80
HA(ATC)TgFBXO1
Plaque area (mm²)
0.6
0.4
0.2
0.0
*
- + - +
TATiΔKu80
HA(ATC)TgFBXO1

Figure 2

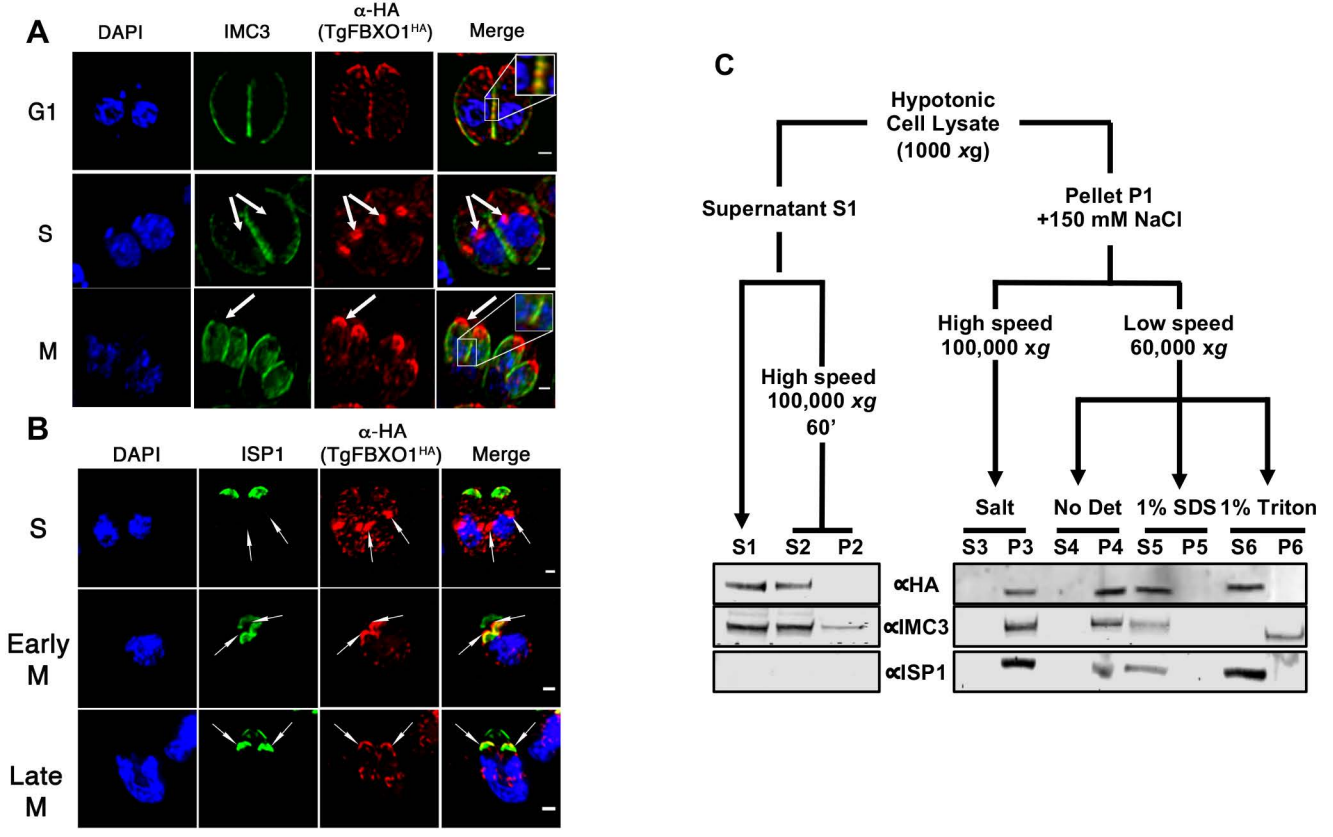
A
DAPI
IMC3
α-HA
(TgFBXO1HA)
Merge
G1
S
M
B
DAPI
ISP1
α-HA
(TgFBXO1HA)
Merge
S
Early M
Late M
C
Hypotonic
Cell Lysate
(1000 xg)
Supernatant S1
Pellet P1
+150 mM NaCl
High speed
100,000 xg
60'
High speed
100,000 xg
Low speed
60,000 xg
Salt
No Det
1% SDS
1% Triton
S1
S2
P2
S3
P3
S4
P4
S5
P5
S6
P6
αHA
αIMC3
αISP1

Figure 3

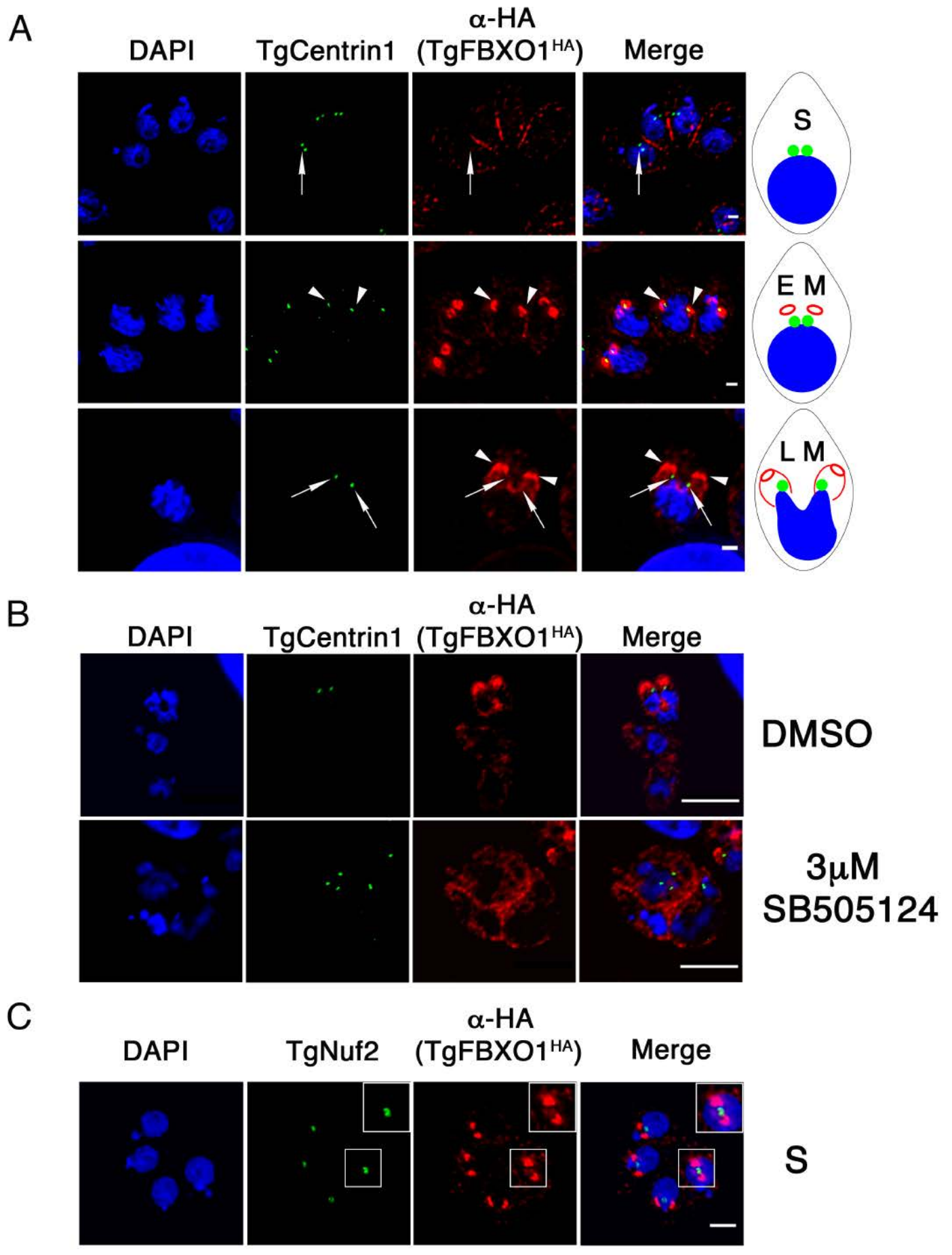
A
DAPI
TgCentrin1
α-HA
(TgFBXO1HA)
Merge
S
E M
L M
B
DAPI
TgCentrin1
α-HA
(TgFBXO1HA)
Merge
DMSO
3μM
SB505124
C
DAPI
TgNuf2
α-HA
(TgFBXO1HA)
Merge
S

Figure 4

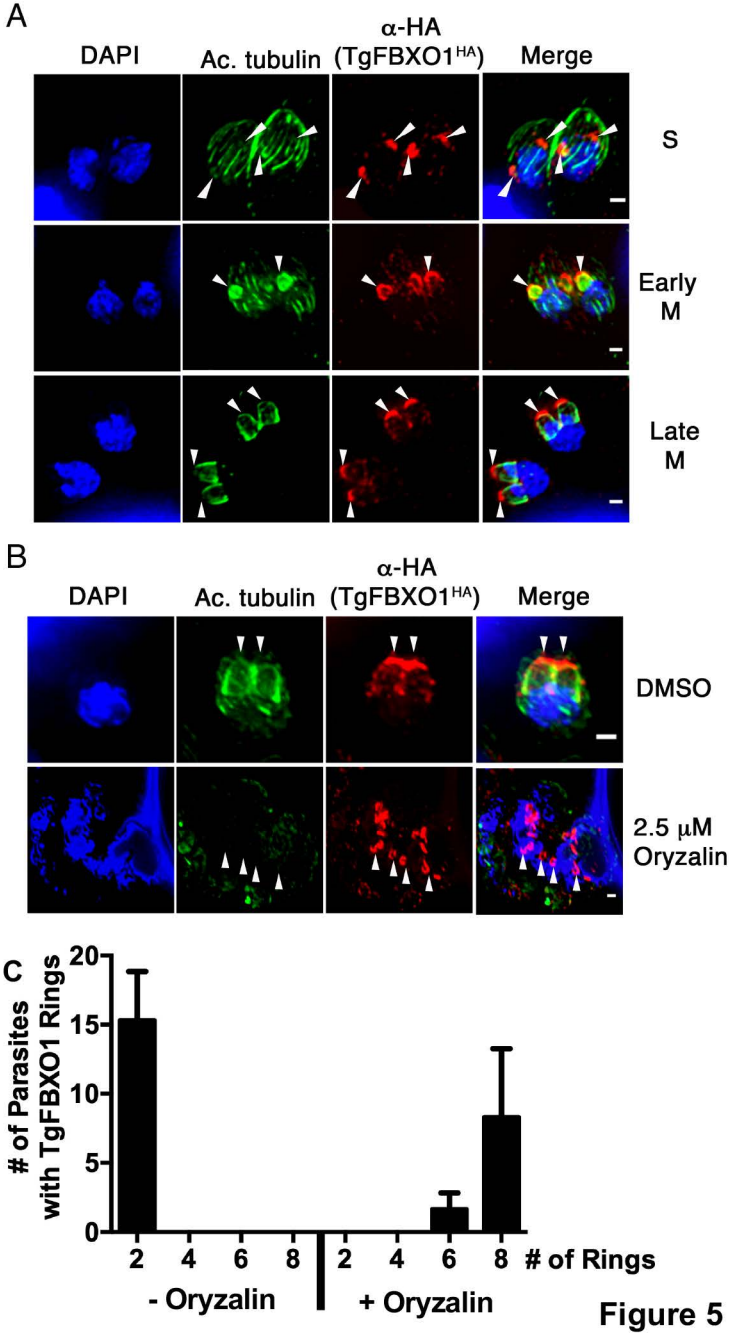
A
DAPI
Ac. tubulin
α-HA (TgFBXO1HA)
Merge
S
Early M
Late M
B
DAPI
Ac. tubulin
α-HA (TgFBXO1HA)
Merge
DMSO
2.5 μM Oryzalin
C
# of Parasites with TgFBXO1 Rings
20
15
10
5
0
2
4
6
8
2
4
6
8
# of Rings
- Oryzalin
+ Oryzalin

Figure 5

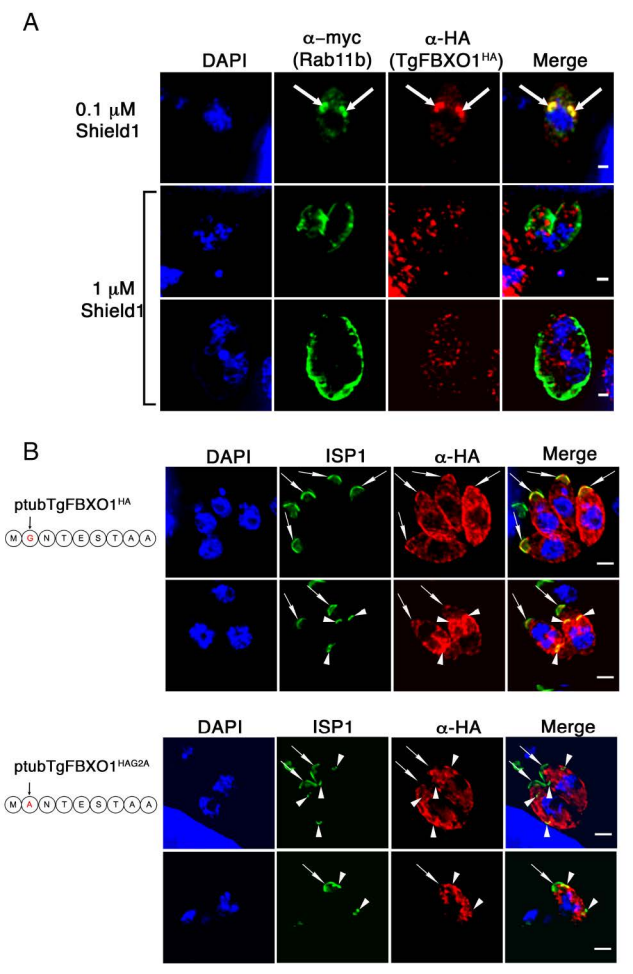
A
DAPI
α–myc (Rab11b)
α-HA (TgFBXO1HA)
Merge
0.1 μM Shield1
1 μM Shield1
B
DAPI
ISP1
α-HA
Merge
ptubTgFBXO1HA
M G N T E S T A A
ptubTgFBXO1HAG2A
M A N T E S T A A

Figure 6

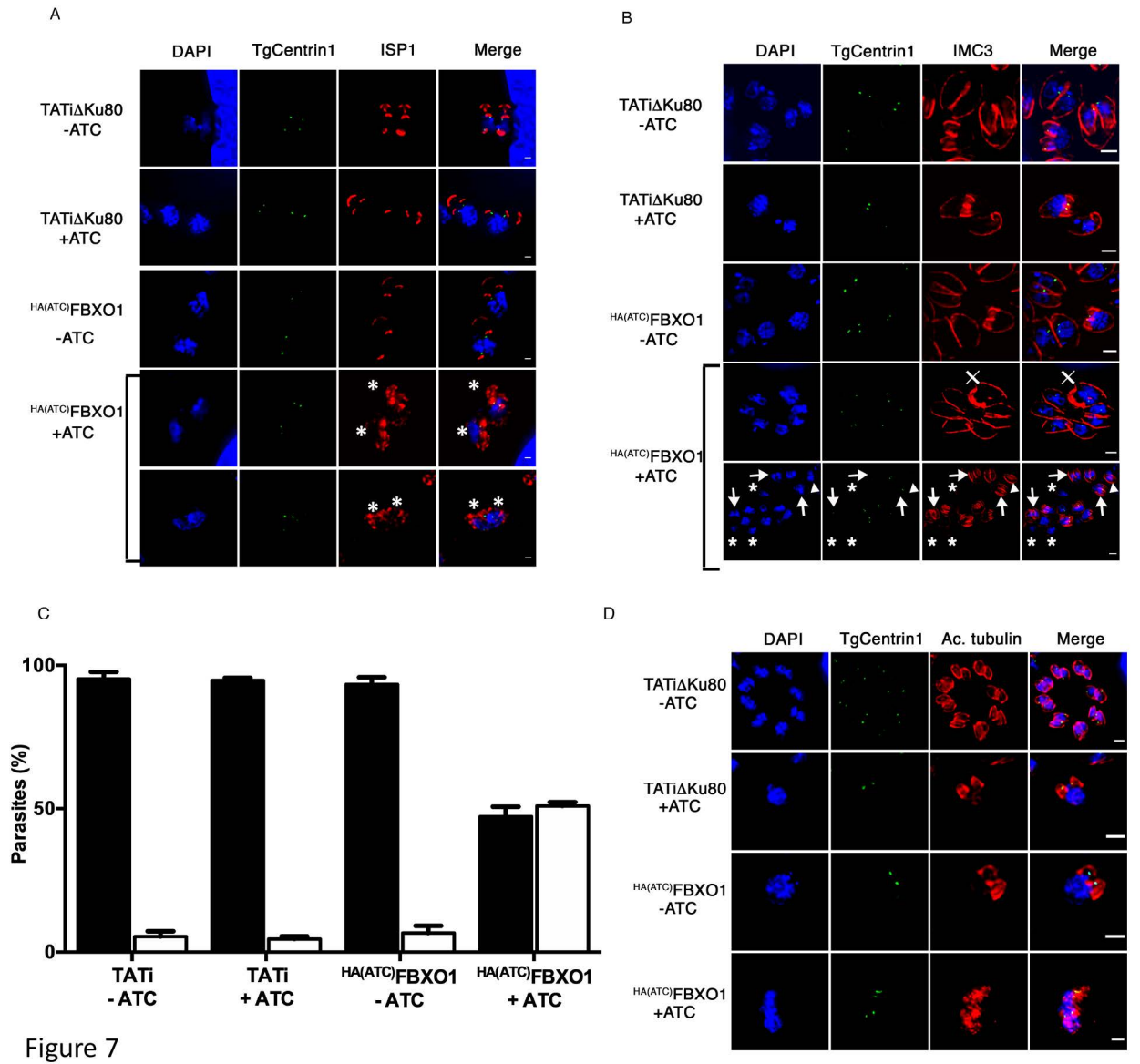
A
DAPI
TgCentrin1
ISP1
Merge
TATiΔKu80 -ATC
TATiΔKu80 +ATC
HA(ATC)FBXO1 -ATC
HA(ATC)FBXO1 +ATC
B
DAPI
TgCentrin1
IMC3
Merge
TATiΔKu80 -ATC
TATiΔKu80 +ATC
HA(ATC)FBXO1 -ATC
HA(ATC)FBXO1 +ATC
C
Parasites (%)
100
50
0
TATi - ATC
TATi + ATC
HA(ATC)FBXO1 - ATC
HA(ATC)FBXO1 + ATC
D
DAPI
TgCentrin1
Ac. tubulin
Merge
TATiΔKu80 -ATC
TATiΔKu80 +ATC
HA(ATC)FBXO1 -ATC
HA(ATC)FBXO1 +ATC

Figure 7